

Pair-checkerboard antiferromagnetic order in β -Fe₄Se₅ with $\sqrt{5} \times \sqrt{5}$ ordered Fe vacancies

Miao Gao¹, Xin Kong², Xun-Wang Yan³, Zhong-Yi Lu^{4,*} and Tao Xiang^{2,5†}

¹*Department of Microelectronics Science and Engineering,
Faculty of Science, Ningbo University, Zhejiang 315211, China*

²*Institute of Physics, Chinese Academy of Sciences, Beijing 100190, China*

³*School of physics and electrical engineering, Anyang Normal University, Henan 455000, China*

⁴*Department of Physics, Renmin University of China, Beijing 100872, China and*

⁵*Collaborative Innovation Center of Quantum Matter, Beijing, China*

(Dated: September 24, 2018)

The electronic structure of recently discovered β -Fe₄Se₅ with $\sqrt{5} \times \sqrt{5}$ ordered Fe vacancies is calculated using first-principles density functional theory. We find that the ground state is an antiferromagnetic (AFM) insulator in agreement with the experimental observation. In K₂Fe₄Se₅, it is known that the ground state is $\sqrt{5} \times \sqrt{5}$ -blocked-checkerboard AFM ordered. But for this material, we find that the ground state is $\sqrt{5} \times \sqrt{5}$ -pair-checkerboard AFM ordered, in which the intrablock four Fe spins exhibit the collinear AFM order and the interblock spins on any two nearest-neighbor sites are antiparallel aligned. This state is about 130 meV/Fe lower in energy than the $\sqrt{5} \times \sqrt{5}$ -blocked-checkerboard AFM one. Electron doping can lower the energy of the $\sqrt{5} \times \sqrt{5}$ -blocked-checkerboard AFM state and introduce a transition between these two states, suggesting that there is strong AFM fluctuation in FeSe-based materials upon doping. This provides a unified picture to understand the AFM orders in β -Fe₄Se₅ and in alkali-metal intercalated FeSe materials.

PACS numbers: 74.70.Xa, 74.20.Mn, 74.20.Pq

I. INTRODUCTION

The discovery of iron-based superconductors has opened a new path to explore unconventional mechanism of high-temperature superconductivity¹. The superconducting transition temperatures of iron-based superconductors are closely related to the height of anion from the Fe-Fe square lattice and the Fe-(As/Se)-Fe angle²⁻⁴. By intercalating atoms between FeSe layers to form $A_{1-x}Fe_{2-y}Se_2$ compounds ($A=K, Tl, Rb, \text{ or } Cs$), one can effectively modulate the height of anion and raise the superconducting transition temperature of bulk FeSe from 8 K⁵ to 27~48 K⁶⁻¹¹.

$A_{1-x}Fe_{2-y}Se_2$ possesses different kinds of Fe-vacancy orders. For example, the two commonly studied $K_{2x}Fe_{2-x}Se_2$ compounds, $K_2Fe_3Se_4$ ($KFe_{1.5}Se_2$) and $K_2Fe_4Se_5$ ($K_{0.8}Fe_{1.6}Se_2$), have the $\sqrt{2} \times 2\sqrt{2}$ and $\sqrt{5} \times \sqrt{5}$ Fe-vacancy orders, respectively. These two compounds were predicted to be AFM semiconductors by the first-principles calculations^{12,13}, and later confirmed by the experimental measurements¹⁴⁻¹⁶. Other kind of Fe-vacancy orders has also been observed¹⁷. The stoichiometric compound KFe_2Se_2 without Fe vacancies is unstable against mesoscopic phase separation¹⁸⁻²¹. But it can be stabilized and become a high- T_c superconductor^{22,23} by proximity to $K_2Fe_4Se_5$.

Recently, a series of β -Fe_{1-x}Se materials without metal intercalations but with Fe vacancies were synthesized. Through the measurement of electron microscopy, Fe vacancies are also found to be ordered and mainly in the phases with $\sqrt{2} \times \sqrt{2}$, $\sqrt{5} \times \sqrt{5}$, and $\sqrt{10} \times \sqrt{10}$ vacancy orders²⁴. It indicates that the Fe-vacancy order is a common feature of FeSe-based superconductors. Fur-

thermore, it was found that most of β -Fe_{1-x}Se samples synthesized in laboratory are in the $\sqrt{5} \times \sqrt{5}$ phase, and the compound with such a vacancy order, i.e. β -Fe₄Se₅, is an AFM insulator^{24,25}. As both β -Fe₄Se₅ and K₂Fe₄Se₅ have the same Fe-vacancy orders, it is interesting to know whether they have the same magnetic order in the ground states.

In this paper, we present the result for the electronic and magnetic structures of β -Fe₄Se₅ with the $\sqrt{5} \times \sqrt{5}$ Fe-vacancy order obtained by the first-principles density functional calculations. We find that β -Fe₄Se₅ is an insulator with a $\sqrt{5} \times \sqrt{5}$ -pair-checkerboard AFM order. In this AFM ordered state, each Fe block contains four Fe spins which are collinear AFM aligned. The band gap of β -Fe₄Se₅ in this $\sqrt{5} \times \sqrt{5}$ -pair-checkerboard AFM phase is found to be 290 meV, in agreement with the experimental observation^{24,25}. This AFM order is stable against light electron doping. It is replaced by the $\sqrt{5} \times \sqrt{5}$ -blocked-checkerboard AFM order (which is also the AFM order observed in K₂Fe₄Se₅) when the doping level exceeds 1.7 electrons per Fe₄Se₅ formula.

II. COMPUTATIONAL DETAILS

In our calculations the plane wave basis method is used²⁶. We adopt the generalized gradient approximation (GGA) of Perdew-Burke-Ernzerhof²⁷ for the exchange-correlation potentials. The ultrasoft pseudopotentials²⁸ are used to model the electron-ion interactions. After full convergence test, the kinetic energy cut-off and the charge density cut-off of the plane wave bases are taken to be 45 Ry and 480 Ry, respectively.

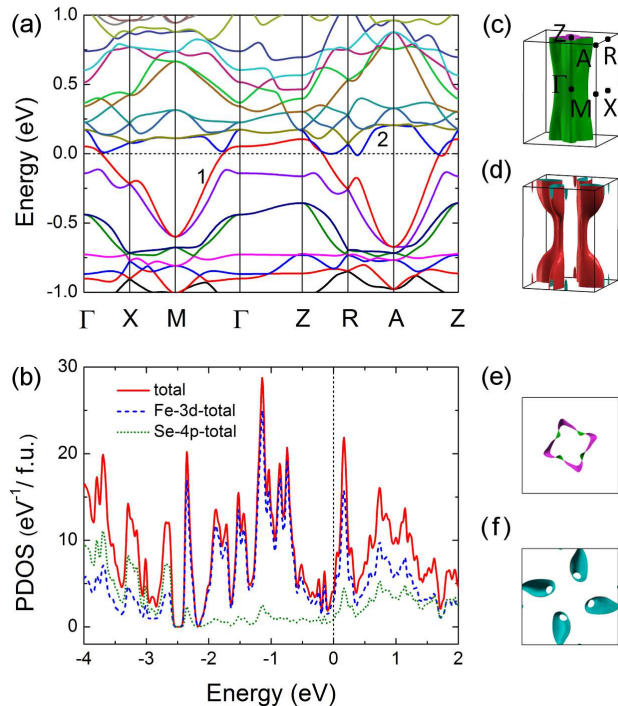


FIG. 1. (Color online) Electronic structures of β - Fe_4Se_5 with the $\sqrt{5} \times \sqrt{5}$ Fe-vacancy order in the nonmagnetic phase. (a) Band structures. The Fermi energy is set to zero. (b) Orbital-resolved partial density of states per formula of β - Fe_4Se_5 . (c) and (d) Fermi surfaces corresponding to the energy bands labelled by the Arabic numbers, 1 and 2, shown in (a), respectively. The high-symmetry points in the Brillouin zone are given in (c). (e) and (f) Top views of the two Fermi surfaces.

Our calculation is done with a $\sqrt{5} \times \sqrt{5} \times 1$ tetragonal unit cell which contains one FeSe layer with 8 Fe atoms, 2 vacancies, and 10 Se atoms. A mesh of $8 \times 8 \times 10$ \mathbf{k} -points is used to sample the Brillouin zone of the $\sqrt{5} \times \sqrt{5} \times 1$ unit cell. The Gaussian broadening technique of width 0.002 Ry is used in the calculation of metallic states. The convergence is tested with a denser $16 \times 16 \times 20$ \mathbf{k} -mesh. There are two degenerate ground states, corresponding to the two degenerate chiral structures of the $\sqrt{5} \times \sqrt{5}$ lattice^{13,29}. We choose the right-chiral structure to do the calculation.

III. RESULTS AND ANALYSIS

For the vacancy ordered β - Fe_4Se_5 , there are eight Fe atoms in each $\sqrt{5} \times \sqrt{5} \times 1$ unit cell. These eight Fe atoms can be divided into two blocks. One block contains the four Fe atoms in the middle of the unit cell enclosed by the blue box as shown in Fig. 2, and the other contains the rest four Fe atoms.

The nonmagnetic (NM) phase of β - Fe_4Se_5 is metallic.

TABLE I. Total energies, averaged magnitudes of the magnetic moments of Fe spins ($|M|$), and band gaps of the ten AFM orders shown in Fig. 2. The energy of NM is set to zero.

AFM states	energy (meV/Fe)	$ M $ (μ_B)	band gap (meV)
AFM- <i>a</i>	-127.4	2.48	0.0
AFM- <i>b</i>	-77.8	2.53	82.6
AFM- <i>c</i>	-188.9	2.72	208.5
AFM- <i>d</i>	-155.5	2.66	163.6
AFM- <i>e</i>	-114.0	2.53	75.7
AFM- <i>f</i>	-245.6	2.70	290.0
AFM- <i>g</i>	-20.3	2.29	0.0
AFM- <i>h</i>	-168.4	2.47	0.0
AFM- <i>i</i>	-207.7	2.66	20.8
AFM- <i>j</i>	-115.8	2.35	0.0

Figure 1 shows the band structure and the partial density of states in the NM state. There are two bands crossing the Fermi level, forming one pillar-shaped hole Fermi surface along the Γ -Z line [Figs. 1(c) and 1(e)] and one windmill-type electron Fermi surfaces around the zone center [Figs. 1(d) and 1(f)]. The low-energy physics is governed by Fe 3d orbitals, since the density of states (DOS) in the energy range from -2.5 eV to 1.0 eV is contributed mainly by Fe 3d electrons.

The ground state, or the lowest energy state, of β - Fe_4Se_5 in the $\sqrt{5} \times \sqrt{5}$ vacancy ordered phase is AFM ordered. In order to determine the magnetic structure of the ground state, we have calculated the electronic structures for all ten non-equivalent AFM states allowed in a $\sqrt{5} \times \sqrt{5}$ lattice. Figure 2 shows the spin configurations of these ten AFM states, labelled from AFM-*a* to AFM-*j*. These states can be divided into three groups, depending on the number of up spins in the middle four Fe atoms, which is called an Fe block, within each unit cell enclosed by the blue square. The first group contains the spin configurations represented by (AFM-*a*)-(AFM-*c*) with just one up spin in an Fe block. The second one consists of the spin configurations represented by (AFM-*d*)-(AFM-*i*) with two up spins in an Fe block. There is one spin configuration, i.e. AFM-*j*, in the third group. It contains four up spins in an Fe block. The AFM states with one and three up Fe spins in an Fe block are energetically degenerate and physically equivalent. The states with two up spins inside an Fe block can have either a collinear AFM order [Figs. 2(d)-(g)] or a checkerboard one [Figs. 2(h) and 2(i)]. Among these states, AFM-*j* is the $\sqrt{5} \times \sqrt{5}$ -blocked-checkerboard AFM order, which is the magnetic order observed in the ground state of $\text{K}_2\text{Fe}_4\text{Se}_5$.

The relative energies of the ten AFM states with respect to the energy of the NM state are given in Table I. The ground state of β - Fe_4Se_5 is that shown in Fig. 2(f), namely the state labelled by AFM-*f*. It is a $\sqrt{5} \times \sqrt{5}$ -pair-checkerboard AFM state. A similar AFM state, called the pair-checkerboard AFM state, was found to be the ground state of bulk β -FeSe based on the first principles

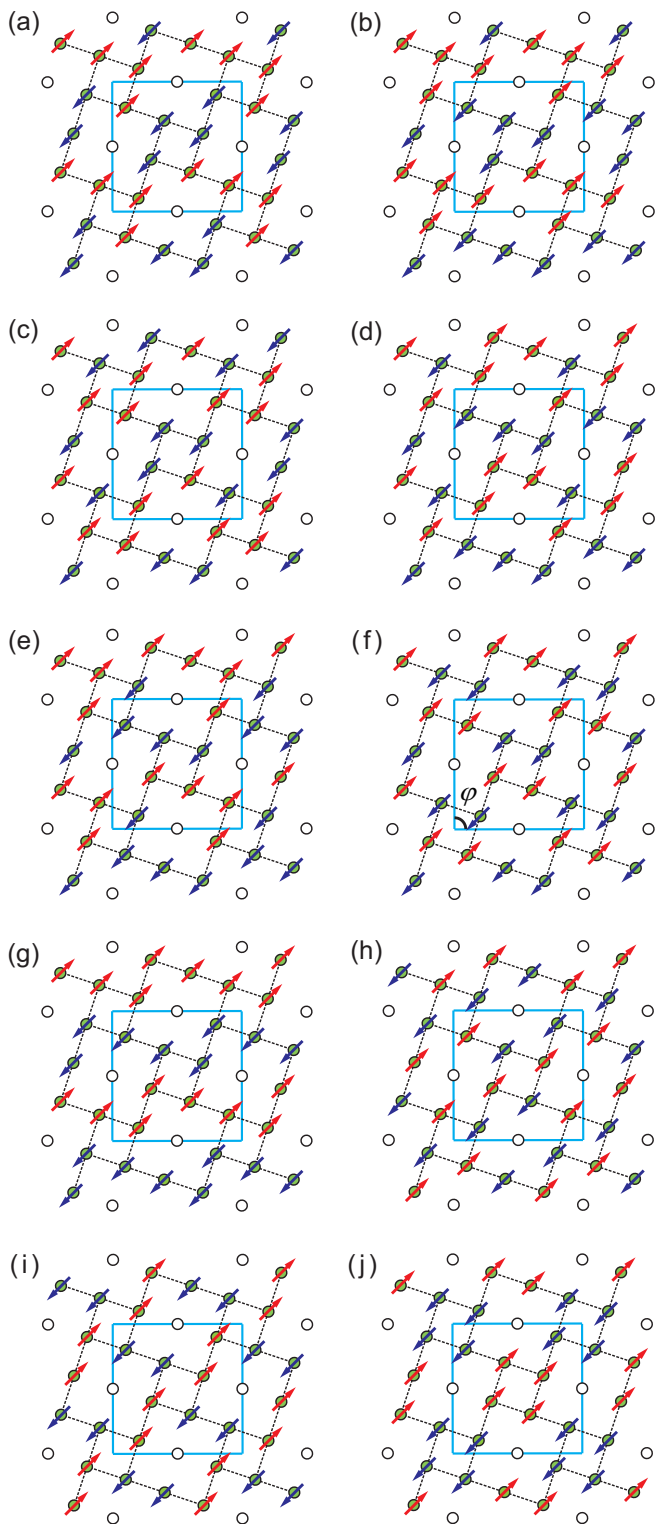


FIG. 2. (Color online) Schematic top views of ten possible AFM orders, labelled from AFM-*a* to AFM-*j*, in each FeSe layer. The $\sqrt{5} \times \sqrt{5}$ -pair-checkerboard AFM order shown in (f) is the magnetic structure for the ground-state of β -Fe₄Se₅. The squares enclosed by the blue lines denote the unit cells. The filled and empty circles represent Fe atoms and Fe vacancies, respectively. The up and down Fe spins are represented by red and blue arrows, respectively.

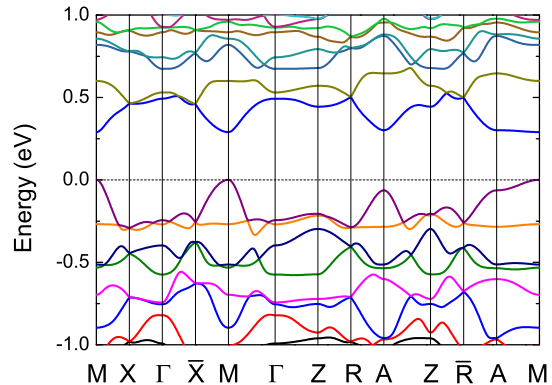


FIG. 3. (Color online) Calculated electronic band structure of β -Fe₄Se₅ in the $\sqrt{5} \times \sqrt{5}$ -pair-checkerboard AFM state with a tetragonal unit cell. The top of the valance band energy is set to zero. The Brillouin zone is the same as that in Fig. 1(c). The fractional coordinates of *X*, \bar{X} , *R* and \bar{R} with respect to the reciprocal lattice vectors are (0.0, 0.5, 0.0), (0.5, 0.0, 0.0), (0.0, 0.5, 0.5) and (0.5, 0.0, 0.5), respectively.

electronic structure calculations³⁰. AFM-*f* can be regarded as a realization of this pair-checkerboard AFM order on the $\sqrt{5} \times \sqrt{5}$ Fe-vacancy ordered lattice.

In the ground state, the lattice undergoes a tetragonal to monoclinic structure transition induced by the spin-lattice interaction. This changes the angle, φ , defined in Fig. 2(f) from 90° to 89.2° with an energy gain of 0.8 meV/Fe. Consequently, there is a tiny difference between the lattice parameters along the *a* and *b* axes, which are equal to 8.4519 Å and 8.4855 Å, respectively. This kind of structure transition is similar to the tetragonal-orthorhombic phase transition observed in other parent compounds of iron-based superconductors^{31–34}.

Figure 3 shows the band structure of β -Fe₄Se₅ in the $\sqrt{5} \times \sqrt{5}$ -pair-checkerboard AFM state obtained with a tetragonal unit cell by ignoring the monoclinic distortion. It indicates clearly that β -Fe₄Se₅ is an AFM insulator with a direct energy gap of about 290 meV, in agreement with the experimental observation^{24,25}.

Figure 4 shows the orbital-resolved partial DOS in the $\sqrt{5} \times \sqrt{5}$ -pair-checkerboard AFM state with tetragonal symmetry. This AFM state is invariant under the following two kinds of transformations: One is to combine an *ab*-plane reflection with a fractional translation of $(-1/2, 1/2, 0)$, the other is to take a spin inversion and then a 180° rotation around the *c*-axis. This symmetry property ensures the spin-up/down DOS at an Fe atom to equal the spin-down/up DOS at the diagonal Fe atom inside the same block. Thus we need only to show the orbital-resolved partial DOS for two Fe atoms, labelled by Fe₁ and Fe₂ in the figure. For Fe₁, the five up-spin orbitals are almost completely filled, but the five down-spin orbitals are only partially filled. The DOS at Fe₂ behaves similarly, but the up and down spins are reversed. The

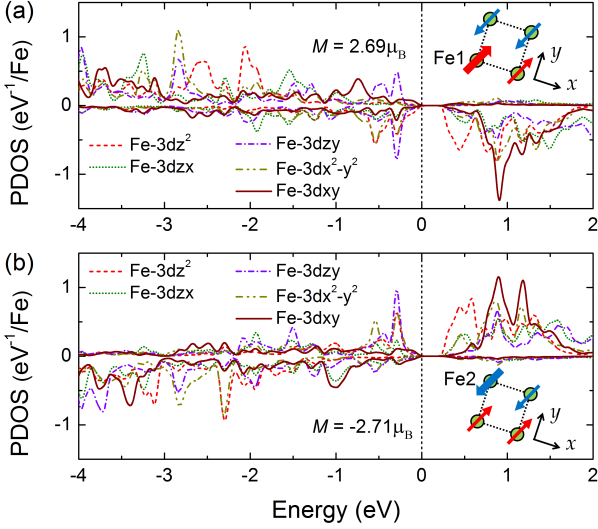


FIG. 4. (Color online) Orbital-resolved partial density of states (PDOS) for the five Fe 3d orbitals at (a) site Fe₁ and (b) site Fe₂ in the $\sqrt{5} \times \sqrt{5}$ -pair-checkerboard AFM state. The spins of Fe₁ and Fe₂ are highlighted by large arrows. The magnetic moments of these two Fe atoms are given in the corresponding figures.

magnetic moment of Fe₂ is slightly larger than that of Fe₁. This leads to the difference in the DOSs between the up/down-spin part of Fe₁ and the down/up-spin one of Fe₂. The unoccupied states are mainly contributed by d_{z^2} and d_{xy} orbitals.

We also find that the AFM states defined by AFM-*b*, AFM-*c*, AFM-*d*, AFM-*e*, and AFM-*i* are insulating. The excitation energy gaps are equal to 82.6 meV, 208.5 meV, 163.6 meV, 75.7 meV, and 20.8 meV, respectively. For AFM-*d*, the band gaps for the up- and down-spin electrons are not equal to each other, since the corresponding up- and down-spin configurations are not equivalent. They equal 163.6 meV and 233.1 meV, respectively. The other AFM states, including the $\sqrt{5} \times \sqrt{5}$ -blocked-checkerboard AFM state, i.e. AFM-*j*, are metallic. This differs from the case in K₂Fe₄Se₅^{12,14,16} where the ground state is blocked-checkerboard AFM ordered but insulating. AFM-*a* is in fact not a truly AFM state, although we initially set the up- and down-spin moments the same in the amplitude in our calculation. But after full optimization, we find that it is actually a ferrimagnetic state with a net magnetization about 1.97 μ_B per unit cell.

In β -Fe₄Se₅, the energy of the $\sqrt{5} \times \sqrt{5}$ -pair-checkerboard AFM state is 129.9 meV/Fe lower than the $\sqrt{5} \times \sqrt{5}$ -blocked-checkerboard AFM one. In contrast, the energy of the former is about 95.8 meV/Fe higher than the latter in K₂Fe₄Se₅. Apparently, the difference results from the intercalation of K atoms in Fe₄Se₅: First, the intercalated K atoms impose a tensile strain on each Fe₄Se₅ layer, which enlarges the *a*-axis lattice constant

from 8.41 Å in β -Fe₄Se₅ to 8.69 Å in K₂Fe₄Se₅. Second, the intercalated atoms dope electrons into Fe₄Se₅ layers.

To understand the effect of tensile strain introduced by K atoms, we calculate the energies of $\sqrt{5} \times \sqrt{5}$ -pair-checkerboard and $\sqrt{5} \times \sqrt{5}$ -blocked-checkerboard AFM states as a function of the *a*-axis lattice constant for β -Fe₄Se₅ with tetragonal unit cell. The lattice constant along the *c*-axis and internal atomic positions are relaxed to minimize the total energy. In a wide range of the *a*-axis lattice constant, as shown in Fig. 5(a), we find that the $\sqrt{5} \times \sqrt{5}$ -pair-checkerboard AFM order is more stable than the $\sqrt{5} \times \sqrt{5}$ -blocked-checkerboard AFM one. It suggests that the difference between β -Fe₄Se₅ and K₂Fe₄Se₅ is not due to the tensile strain effect.

To understand the charge doping effect, we introduce extra electrons to β -Fe₄Se₅ and to K₂Fe₄Se₅ with all K atoms removed (namely, K₂Fe₄Se₅-2K). A jellium background with positive charge is introduced to compensate the doped electrons and to avoid numerical divergence in the calculation. Note that different AFM states have different optimized lattice constants. For example, the optimized lattice constants are $a=8.4682$ Å and $c=6.5241$ Å in the $\sqrt{5} \times \sqrt{5}$ -pair-checkerboard AFM state, and $a=8.1092$ Å and $c=6.2119$ Å in the $\sqrt{5} \times \sqrt{5}$ -blocked-checkerboard AFM order of β -Fe₄Se₅. In order to avoid the complication introduced by the lattice parameters, we do the calculation by taking the experimental lattice constants, i.e., $a=8.41$ Å and $c=5.47$ Å for β -Fe₄Se₅²⁴,

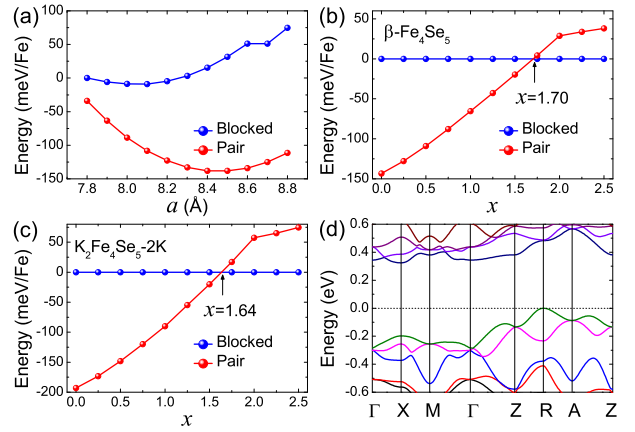


FIG. 5. (Color online) Comparison between the $\sqrt{5} \times \sqrt{5}$ -pair-checkerboard AFM and the $\sqrt{5} \times \sqrt{5}$ -blocked-checkerboard AFM states. (a) Total energies of these two AFM orders in β -Fe₄Se₅ as functions of the *a*-axis lattice constant with tetragonal unit cell. The energy of the $\sqrt{5} \times \sqrt{5}$ -blocked-checkerboard AFM state at $a=7.8$ Å is set to zero. (b) Relative energy of the $\sqrt{5} \times \sqrt{5}$ -pair-checkerboard AFM state (red) with respect to the $\sqrt{5} \times \sqrt{5}$ -blocked-checkerboard AFM state (blue) as a function of doped electron concentration x for β -Fe₄Se₅. (c) Same as in (b) but for K₂Fe₄Se₅-2K. (d) Band structure of the $\sqrt{5} \times \sqrt{5}$ -blocked-checkerboard AFM state in the electron doped β -Fe₄Se₅ with $x=2$.

$a=8.6929 \text{ \AA}$ and $c=14.0168 \text{ \AA}$ for $\text{K}_2\text{Fe}_4\text{Se}_5\text{-}2\text{K}^{14}$.

For both materials without electron doping, we find that the $\sqrt{5} \times \sqrt{5}$ -pair-checkerboard AFM state is lower in energy than the $\sqrt{5} \times \sqrt{5}$ -blocked-checkerboard one [Figs. 5(b) and 5(c)]. Upon electron doping, the energy difference between these two states gradually decreases. A reversion in the total energy happens at a critical doping roughly equal to 1.7 electrons per formula for both $\beta\text{-Fe}_4\text{Se}_5$ and $\text{K}_2\text{Fe}_4\text{Se}_5\text{-}2\text{K}$. The $\sqrt{5} \times \sqrt{5}$ -blocked-checkerboard AFM state is 57.5 meV/Fe lower than the $\sqrt{5} \times \sqrt{5}$ -pair-checkerboard one by adding 2 electrons per formula to $\text{K}_2\text{Fe}_4\text{Se}_5\text{-}2\text{K}$. Here $\text{K}_2\text{Fe}_4\text{Se}_5\text{-}2\text{K}+2e$ is isoelectronic to $\text{K}_2\text{Fe}_4\text{Se}_5$. Thus adding electron to Fe_4Se_5 layers reproduces correctly the ground-state AFM order of $\text{K}_2\text{Fe}_4\text{Se}_5$. It suggests that the difference in the magnetic orders between $\beta\text{-Fe}_4\text{Se}_5$ and $\text{K}_2\text{Fe}_4\text{Se}_5$ results mainly from the doping effect introduced by the intercalated K atoms. Furthermore, by doping 2 electrons per formula to $\beta\text{-Fe}_4\text{Se}_5$, we find that the metallic $\sqrt{5} \times \sqrt{5}$ -blocked-checkerboard AFM state becomes insulating, with an energy gap of 324 meV [Fig. 5(d)]. This is reminiscent of the insulating AFM state of $\text{K}_2\text{Fe}_4\text{Se}_5$ ¹³.

With the increase of electron doping, we find that the nearest-neighboring Fe-Fe bond length inside the inner Fe block decreases. This leads to a tetramer lattice distortion of Fe atoms, in both the $\sqrt{5} \times \sqrt{5}$ -blocked-checkerboard and the $\sqrt{5} \times \sqrt{5}$ -pair-checkerboard AFM states. The tetramer distortion also exists in the ground state of $\text{K}_2\text{Fe}_4\text{Se}_5$ ¹³. It is in fact this tetramer distortion that stabilizes the $\sqrt{5} \times \sqrt{5}$ -blocked-checkerboard AFM order in $\text{K}_2\text{Fe}_4\text{Se}_5$. To check how important this effect is in $\beta\text{-Fe}_4\text{Se}_5$, we carry out a total-energy calculation for this material without any tetramer distortion by using the lattice parameters obtained from the bulk $\beta\text{-FeSe}$. We find that the $\sqrt{5} \times \sqrt{5}$ -blocked-checkerboard AFM state is about 27.8 meV/Fe higher in energy than the $\sqrt{5} \times \sqrt{5}$ -pair-checkerboard one at the doping of

2 electrons per Fe_4Se_5 formula. This shows that it is the tetramer lattice distortion enhanced by electron doping that lowers the energy of the $\sqrt{5} \times \sqrt{5}$ -blocked-checkerboard AFM state.

The above results are obtained without considering the van der Waals (vdW) interaction between FeSe layers. This overestimates the lattice constant along the c -axis. If the vdW correction^{35,36} is taken into account, we find that the ground state is still $\sqrt{5} \times \sqrt{5}$ -pair-checkerboard AFM insulator. The band gap is 172 meV, and the a - and c -axis lattice constants are respectively 8.2440 \AA and 5.5619 \AA , in agreement with the experimental results²⁴.

IV. SUMMARY

In conclusion, we have studied the electronic and magnetic structures of $\beta\text{-Fe}_4\text{Se}_5$. Similar to $\text{K}_2\text{Fe}_4\text{Se}_5$, we find that the ground state of $\beta\text{-Fe}_4\text{Se}_5$ is an AFM insulator. But the ground-state is $\sqrt{5} \times \sqrt{5}$ -pair-checkerboard AFM ordered, unlike in $\text{K}_2\text{Fe}_4\text{Se}_5$ where the ground state is $\sqrt{5} \times \sqrt{5}$ -blocked-checkerboard AFM ordered. The band excitation gap of $\beta\text{-Fe}_4\text{Se}_5$ is 290 meV, in agreement with the experimental result. The $\sqrt{5} \times \sqrt{5}$ -pair-checkerboard AFM order is robust against the lattice tensile strain. But electron doping, introduced by extra Fe or intercalated alkali-metal atoms, can turn it into a $\sqrt{5} \times \sqrt{5}$ -blocked-checkerboard AFM state above a critical doping level.

ACKNOWLEDGMENTS

This work is supported by National Natural Science Foundation of China (Grant Nos. 11404383, 91421304, 11474331, and 11474004). M.G. is also supported by Zhejiang Provincial Natural Science Foundation of China under Grant No. LY17A040005 and K.C.Wong Magna Fund in Ningbo University.

* zlu@ruc.edu.cn

† txiang@iphy.ac.cn

¹ Y. Kamihara, T. Watanabe, M. Hirano, and H. Hosono, *Iron-Based Layered Superconductor $\text{La}[\text{O}_{1-x}\text{F}_x]\text{FeAs}$ ($x=0.05\text{-}0.12$) with $T_c=26 \text{ K}$* , J. Am. Chem. Soc. **130**, 3296 (2008).

² J. Zhao, Q. Huang, C. de la Cruz, S. Li, J. W. Lynn, Y. Chen, M. A. Green, G. F. Chen, G. Li, Z. Li, J. L. Luo, N. L. Wang, and P. Dai, *Structural and magnetic phase diagram of $\text{CeFeAsO}_{1-x}\text{F}_x$ and its relation to high-temperature superconductivity*, Nat. Mater. **7**, 953 (2008).

³ H. Okabe, N. Takeshita, K. Horigane, T. Muranaka, and J. Akimitsu, *Pressure-induced high- T_c superconducting phase in FeSe : Correlation between anion height and T_c* , Phys. Rev. B **81**, 205119 (2010).

⁴ Y. Mizuguchi, Y. Hara, K. Deguchi, S. Tsuda, T. Yamaguchi, K. Takeda, H. Kotegawa, H. Tou, and Y. Takano,

Anion height dependence of T_c for the Fe-based superconductor, Supercond. Sci. Technol. **23**, 054013 (2010).

⁵ F.-C. Hsu, J.-Y. Luo, K.-W. Yeh, T.-K. Chen, T.-W. Huang, P. M. Wu, Y.-C. Lee, Y.-L. Huang, Y.-Y. Chu, D.-C. Yan, and M.-K. Wu, *Superconductivity in the PbO -type structure $\alpha\text{-FeSe}$* , Proc. Natl. Acad. Sci. U.S.A. **105**, 14262 (2008).

⁶ J. Guo, S. Jin, G. Wang, S. Wang, K. Zhu, T. Zhou, M. He, and X. Chen, *Superconductivity in the iron selenide $\text{K}_x\text{Fe}_2\text{Se}_2$ ($0 \leq x \leq 1.0$)*, Phys. Rev. B **82**, 180520(R) (2010).

⁷ A. Krzton-Maziopa, Z. Shermadini, E. Pomjakushina, V. Pomjakushin, M. Bendele, A. Amato, R. Khasanov, H. Luetkens, and K. Conder, *Synthesis and crystal growth of $\text{Cs}_{0.8}(\text{FeSe}_{0.98})_2$: a new iron-based superconductor with $T_c = 27 \text{ K}$* , J. Phys. Condens. Matter **23**, 052203 (2011).

⁸ M.-H. Fang, H.-D. Wang, C.-H. Dong, Z.-J. Li, C.-M. Feng, J. Chen, and H. Q. Yuan, *Fe-based superconductivity*

- with $T_c=31K$ bordering an antiferromagnetic insulator in $(Tl,K)Fe_xSe_2$, *Europhys. Lett.* **94**, 27009 (2011).
- ⁹ H.-D. Wang, C.-H. Dong, Z.-J. Li, Q.-H. Mao, S.-S. Zhu, C.-M. Feng, H. Q. Yuan, and M.-H. Fang, *Superconductivity at 32 K and anisotropy in $Tl_{0.58}Rb_{0.42}Fe_{1.72}Se_2$ crystals*, *Europhys. Lett.* **93**, 47004 (2011).
 - ¹⁰ L. Sun, X.-J. Chen, J. Guo, P. Gao, Q.-Z. Huang, H. Wang, M. Fang, X. Chen, G. Chen, Q. Wu, C. Zhang, D. Gu, X. Dong, L. Wang, K. Yang, A. Li, X. Dai, H.-k. Mao, and Z. Zhao, *Re-emerging superconductivity at 48 kelvin in iron chalcogenides*, *Nature* **483**, 67 (2012).
 - ¹¹ T. P. Ying, X. L. Chen, G. Wang, S. F. Jin, T. T. Zhou, X. F. Lai, H. Zhang and W. Y. Wang, *Observation of superconductivity at 30~46K in $A_xFe_2Se_2$ ($A=Li, Na, Ba, Sr, Ca, Yb, and Eu$)*, *Sci. Rep.* **2**, 426 (2012).
 - ¹² X.-W. Yan, M. Gao, Z.-Y. Lu, and T. Xiang, *Electronic Structures and Magnetic Order of Ordered-Fe-Vacancy Ternary Iron Selenides $TlFe_{1.5}Se_2$ and $AFe_{1.5}Se_2$ ($A=K, Rb, or Cs$)*, *Phys. Rev. Lett.* **106**, 087005 (2011).
 - ¹³ X.-W. Yan, M. Gao, Z.-Y. Lu, and T. Xiang, *Ternary iron selenide $K_{0.8}Fe_{1.6}Se_2$ is an antiferromagnetic semiconductor*, *Phys. Rev. B* **83**, 233205 (2011).
 - ¹⁴ W. Bao, Q. Huang, G. F. Chen, M. A. Green, D. M. Wang, J. B. He, X. Q. Wang, and Y. Qiu, *A Novel Large Moment Antiferromagnetic Order in $K_{0.8}Fe_{1.6}Se_2$ Superconductor*, *Chin. Phys. Lett.* **28**, 086104 (2011).
 - ¹⁵ J. Zhao, H. Cao, E. Bourret-Courchesne, D.-H. Lee, and R. J. Birgeneau, *Neutron-Diffraction Measurements of an Antiferromagnetic Semiconducting Phase in the Vicinity of the High-Temperature Superconducting State of $K_xFe_{2-y}Se_2$* , *Phys. Rev. Lett.* **109**, 267003 (2012).
 - ¹⁶ F. Chen, M. Xu, Q. Q. Ge, Y. Zhang, Z. R. Ye, L. X. Yang, Juan Jiang, B. P. Xie, R. C. Che, M. Zhang, A. F. Wang, X. H. Chen, D. W. Shen, J. P. Hu, and D. L. Feng, *Electronic Identification of the Parental Phases and Mesoscopic Phase Separation of $K_xFe_{2-y}Se_2$ Superconductors*, *Phys. Rev. X* **1**, 021020 (2011).
 - ¹⁷ X. Ding, D. Fang, Z. Wang, H. Yang, J. Liu, Q. Deng, G. Ma, C. Meng, Y. Hu, and H.-H. Wen, *Influence of microstructure on superconductivity in $K_xFe_{2-y}Se_2$ and evidence for a new parent phase $K_2Fe_7Se_8$* , *Nat. Commun.* **4**, 1897 (2013).
 - ¹⁸ V. Y. Pomjakushin, A. Krzton-Maziopa, E. V. Pomjakushina, K. Conder, D. Chernyshov, V. Svitlyk, and A. Bosak, *Intrinsic crystal phase separation in the antiferromagnetic superconductor $Rb_yFe_{2-x}Se_2$: a diffraction study*, *J. Phys.: Condens. Matter* **24**, 435701 (2012).
 - ¹⁹ A. Ricci, N. Poccia, G. Campi, B. Joseph, G. Arrighetti, L. Barba, M. Reynolds, M. Burghammer, H. Takeya, Y. Mizuguchi, Y. Takano, M. Colapietro, N. L. Saini, and A. Bianconi, *Nanoscale phase separation in the iron chalcogenide superconductor $K_{0.8}Fe_{1.6}Se_2$ as seen via scanning nanofocused x-ray diffraction*, *Phys. Rev. B* **84**, 060511(R) (2011).
 - ²⁰ A. Ricci, N. Poccia, B. Joseph, D. Innocenti, G. Campi, A. Zozulya, F. Westermeier, A. Schavkan, F. Coneri, A. Bianconi, H. Takeya, Y. Mizuguchi, Y. Takano, T. Mizokawa, M. Sprung, and N. L. Saini, *Direct observation of nanoscale interface phase in the superconducting chalcogenide $K_xFe_{2-y}Se_2$ with intrinsic phase separation*, *Phys. Rev. B* **91**, 020503(R) (2015).
 - ²¹ Z. Wang, Y. J. Song, H. L. Shi, Z. W. Wang, Z. Chen, H. F. Tian, G. F. Chen, J. G. Guo, H. X. Yang, and J. Q. Li, *Microstructure and ordering of iron vacancies in the superconductor system $K_yFe_xSe_2$ as seen via transmission electron microscopy*, *Phys. Rev. B* **83**, 140505 (2011).
 - ²² W. Li, H. Ding, Z. Li, P. Deng, K. Chang, K. He, S. Ji, L. Wang, X. Ma, J.-P. Hu, X. Chen, and Q.-K. Xue, *KFe_2Se_2 is the Parent Compound of K-Doped Iron Selenide Superconductors*, *Phys. Rev. Lett.* **109**, 057003 (2012).
 - ²³ G. M. Zhang, Z. Y. Lu, T. Xiang, *Superconductivity mediated by the antiferromagnetic spin-wave in chalcogenide iron-base superconductors*, *Phys. Rev. B* **84**, 052502 (2011).
 - ²⁴ T.-K. Chen, C.-C. Chang, H.-H. Chang, A.-H. Fang, C.-H. Wang, W.-H. Chao, C.-M. Tseng, Y.-C. Lee, Y.-R. Wu, M.-H. Wen, H.-Y. Tang, F.-R. Chen, M.-J. Wang, M.-K. Wu, and D. V. Dyck, *Fe-vacancy order and superconductivity in tetragonal β - $Fe_{1-x}Se$* , *Proc. Natl. Acad. Sci. USA* **111**, 63 (2014).
 - ²⁵ Y. Fang, D. H. Xie, W. Zhang, F. Chen, W. Feng, B. P. Xie, D. L. Feng, X. C. Lai, and S. Y. Tan, *Tunable Fe-vacancy disorder-order transition in $FeSe$ thin films*, *Phys. Rev. B* **93**, 184503 (2016).
 - ²⁶ P. Giannozzi *et al.*, *QUANTUM ESPRESSO: a modular and open-source software project for quantum simulations of materials*, *J. Phys.: Condens. Matter* **21**, 395502 (2009).
 - ²⁷ J. P. Perdew, K. Burke, and M. Ernzerhof, *Generalized Gradient Approximation Made Simple*, *Phys. Rev. Lett.* **77**, 3865 (1996).
 - ²⁸ D. Vanderbilt, *Soft self-consistent pseudopotentials in a generalized eigenvalue formalism*, *Phys. Rev. B* **41**, 7892 (1990).
 - ²⁹ H. Sabrowsky, M. Rosenberg, D. Welz, P. Deppe, and W. Schäfer, *A neutron and Mössbauer study of $TlFe_xS_2$ compounds*, *J. Magn. Magn. Mater.* **54-57**, 1497 (1986).
 - ³⁰ H.-Y. Cao, S. Chen, H. Xiang, X.-G. Gong, *Antiferromagnetic ground state with pair-checkerboard order in $FeSe$* , *Phys. Rev. B* **91**, 020504(R) (2015).
 - ³¹ C. de la Cruz, Q. Huang, J. W. Lynn, J. Li, W. Ratcliff II, J. L. Zarestky, H. A. Mook, G. F. Chen, J. L. Luo, N. L. Wang, P. Dai, *Magnetic order close to superconductivity in the iron-based layered $LaO_{1-x}F_xFeAs$ systems*, *Nature* **453**, 899 (2008).
 - ³² M. Rotter, M. Tegel, D. Johrendt, I. Schellenberg, W. Hermes, and R. Pöttgen, *Spin-density-wave anomaly at 140 K in the ternary iron arsenide $BaFe_2As_2$* , *Phys. Rev. B* **78**, 020503(R) (2008).
 - ³³ T. M. McQueen, A. J. Williams, P. W. Stephens, J. Tao, Y. Zhu, V. Ksenofontov, F. Casper, C. Felser, and R. J. Cava, *Tetragonal-to-Orthorhombic Structural Phase Transition at 90 K in the Superconductor $Fe_{1.01}Se$* , *Phys. Rev. Lett* **103**, 057002 (2009).
 - ³⁴ F. Ma, W. Ji, J. Hu, Z.-Y. Lu, and T. Xiang, *First-Principles Calculations of the Electronic Structure of Tetragonal α - $FeTe$ and α - $FeSe$ Crystals: Evidence for a Bicolinear Antiferromagnetic Order*, *Phys. Rev. Lett.* **102**, 177003 (2009).
 - ³⁵ S. Grimme, *Semiempirical GGA-type density functional constructed with a long-range dispersion correction*, *J. Comp. Chem.* **27**, 1787 (2006).
 - ³⁶ V. Barone, M. Casarin, D. Forrer, M. Pavone, M. Sambri, and A. Vittadini, *Role and effective treatment of dispersive forces in materials: Polyethylene and graphite crystals as test cases*, *J. Comp. Chem.* **30**, 934 (2009).